Open Journal of Physiology and Pharmacology, (2026), Vol. 1(1): 39-51
Case Report
DOI: *10.5455/OJPP.2026.v1.i1.5*

Eldaghayes Publisher
دار الدغيس للنشر
Advancing Knowledge Through Peer-Reviewed Science

Eldaghayes Publisher
www.eldaghayes.com

Submitted: 12/12/2025 Revised: 05/02/2026 Accepted: 17/02/2026 Published: 05/05/2026

Multi-organ pharmacophysiological failure associated with PFAS in the endangered Persian leopard *(Panthera pardus tulliana)*: Single-cell and spatial mapping of mitochondrial, neuroendocrine, and immunometabolic disruption

Peyman Mohammadzadeh[1*], Amin Pilvaieh[1], Mohammad Reza Salim Bahrami[1], Farshad Ziaee[2] and Arshia Dousti[1]

[1]*Department of Pathology, Sa. C. Islamic Azad University, Sanandaj, Iran*
[2]*Student Research Committee, Tabriz University of Medical Sciences, Tabriz, Iran*

ABSTRACT

Background: Per- and polyfluoroalkyl substances (PFASs) are long-lasting environmental pollutants that accumulate in apex predators. The mechanistic consequences of PFAS exposure in endangered large felids remain poorly characterized.

Aim: This study aimed to characterize molecular and pathological features consistent with PFAS-associated multi-organ injury in the endangered Persian leopard (*Panthera pardus tulliana*) using integrative molecular and pathological approaches.

Methods: A complete necropsy was performed on a deceased wild adult male Persian leopard (*P. pardus tulliana*) with clinical signs consistent with multi-organ dysfunction. Tissues from the adrenal cortex, myocardium, renal cortex, liver, and hypothalamus were analyzed using single-cell RNA sequencing, spatial transcriptomics (10x Genomics Visium), transmission electron microscopy, targeted PFAS quantification (LC-MS/MS), high-resolution mitochondrial respirometry, targeted steroidomics, and immunohistochemistry.

Results: Elevated perfluorooctane sulfonate (PFAS) concentrations were detected across all examined tissues, with PFOS as the predominant congener. Ultrastructural analysis revealed severe mitochondrial damage characterized by cristolysis, membrane rupture, and intramitochondrial vacuolation, accompanied by a 57% reduction in oxidative phosphorylation capacity. Spatial transcriptomics demonstrated coordinated downregulation of steroidogenic and oxidative phosphorylation gene networks, spatially juxtaposed with IL18, TNF, and CCL20-expressing inflammatory microdomains. Single-cell profiling identified 31 transcriptional clusters. Steroidogenic cell populations exhibited reduced mitochondrial gene expression, whereas T-cell subsets showed increased expression of inhibitory checkpoint receptors (PDCD1, LAG3, TIGIT, and CTLA4), suggesting immune exhaustion. Targeted steroidomics revealed marked suppression of cortisol, corticosterone, aldosterone, and pregnenolone levels. Immunohistochemistry confirmed reduced mitochondrial mass, impaired mitophagic flux, and elevated oxidative DNA damage.

Conclusion: To the best of our knowledge, this study provides the first detailed molecular and pathological characterization of PFAS-associated multi-organ injury in an endangered large felid. Convergent disruption of mitochondrial, endocrine, and immunometabolic pathways is identified as a key feature associated with PFAS accumulation, with implications for conservation toxicology and wildlife health assessment.

Keywords: PFAS, Persian leopard, *Panthera pardus tulliana*, Mitochondrial dysfunction, Spatial transcriptomics, Immunometabolic disruption.

Introduction

Globally, persistent environmental contaminants are increasingly recognized as major drivers of wildlife morbidity and population decline. Among these, per- and polyfluoroalkyl substances (PFAS) represent a particularly concerning class of pollutants due to their extreme chemical stability, global distribution, and long biological persistence. PFAS resist environmental degradation and exhibit strong affinity for circulating and intracellular proteins—most notably serum albumin, liver fatty acid–binding proteins, and hormone-transport proteins—resulting in prolonged tissue retention and chronic toxic potential (Taher and Lohmann, 2025). Although extensive toxicological data exist from experimental models and selected wildlife species, the cellular and molecular consequences of PFAS exposure in endangered terrestrial carnivores,

***Corresponding Author:** Peyman Mohammadzadeh, Department of Pathology, Sa. C. Islamic Azad University, Sanandaj, Iran. Email: *pathology@iau.ir*

Articles published in Open Journal of Physiology and Pharmacology are licensed under a Creative Commons Attribution-NonCommercial 4.0 International License

particularly in long-lived apex predators such as large felids.

The Persian leopard (*Panthera pardus tulliana*), the largest remaining felid in Western Asia, is currently threatened by habitat fragmentation, human–wildlife conflict, and declining prey availability. Superimposed on these pressures is the increasing environmental chemical pollution burden. As an apex predator occupying the highest trophic levels, the Persian leopard is especially susceptible to bioaccumulative contaminants that enter ecosystems through industrial discharge, persist in soil and water, biomagnify through prey species, and ultimately concentrate in top predators. In carnivores, PFAS exposure is driven predominantly by dietary intake, followed by extensive protein binding rather than exclusive lipid sequestration, leading to long biological half-lives in metabolically active organs such as the liver, kidney, and endocrine tissues. Although PFAS accumulation and toxicity have been well documented in marine mammals, birds of prey, and aquatic food webs, mechanistic data for terrestrial apex predators, particularly large felids, are strikingly limited (Suski, 2020). This gap constrains mechanistic understanding and evidence-based conservation interventions.

Experimental and clinical studies in laboratory animals and humans have demonstrated that PFAS exposure is associated with mitochondrial membrane disruption, impaired fatty acid β-oxidation, inhibition of oxidative phosphorylation (OXPHOS), and increased oxidative stress. PFAS have also been shown to interfere with key regulatory pathways, including peroxisome proliferator–activated receptor alpha (PPAR-α) signaling and glucocorticoid receptor activity, with downstream effects on steroidogenesis and endocrine homeostasis (Fritsche *et al.*, 2023). Emerging evidence further implicates PFAS in neuroendocrine dysregulation, immune modulation, and progressive immunometabolic exhaustion following chronic exposure (Schwarzlmueller *et al.*, 2025). However, these mechanistic insights are largely derived from controlled laboratory systems, and their relevance to endangered wildlife species experiencing lifelong, environmentally realistic exposures remains insufficiently explored.

Importantly, no previous study has integrated high-resolution single-cell transcriptomics, spatial tissue mapping, ultrastructural pathology, endocrine metabolomics, and immunometabolic profiling to examine PFAS-associated pathology in a large felid that is endangered. Such integrative approaches are particularly valuable in wildlife research, where biological replication is rarely feasible, and each specimen represents an irreplaceable source of information.

To address this knowledge gap, this study investigates a single postmortem case of a wild Persian leopard (*Panthera pardus tulliana*) recovered from an industrially contaminated region with documented exposure to PFAS. This work adopts an in-depth, systems-level case-study framework to characterize molecular, cellular, and organ-level alterations consistent with PFAS-associated toxicophysiological disruption rather than establishing causality. By combining conventional diagnostic pathology with PFAS quantification, ultrastructural analysis, single-cell and spatial transcriptomics, steroid hormone profiling, and immune–metabolic mapping, we aimed to reconstruct potential links between chemical burden, cellular dysfunction, and multi-organ pathology within the constraints of a single-specimen design (Mohammadzadeh *et al.*, 2025).

Using this integrative approach, we aim to identify convergent molecular vulnerabilities that may underlie reduced physiological resilience in exposed apex predators. We emphasize that the single-case design precludes definitive causal attribution of all observed alterations solely to PFAS exposure. Therefore, the findings should be interpreted as a detailed molecular and pathological characterization of a potentially PFAS-affected individual. Ultimately, this study aims to bridge experimental toxicology and conservation medicine by providing a mechanistically informed reference framework for interpreting PFAS exposure in endangered terrestrial carnivores, while explicitly acknowledging the limitations inherent to post-mortem, single-animal investigations.

Materials and Methods

Study approval, necropsy, and sampling strategy

We investigated a free-ranging adult male Persian leopard (*P. pardus tulliana*) that was found dead in a mountainous region of northern Iran with documented environmental PFAS contamination. The institutional wildlife ethics committee approved all procedures (Protocol No. WEC-IR-2025). Based on the carcass condition, ambient temperature, rigor mortis, and absence of advanced autolysis, the postmortem interval was estimated to be 4 hours at the time of examination. A complete diagnostic necropsy was initiated within this interval to minimize biomolecule postmortem degradation. All procedures were conducted under a Class II biosafety cabinet to ensure the safety of the operator and sample integrity (Sarri *et al.*, 2025).

Comprehensive tissue sampling was performed under sterile conditions, including the liver, kidney (cortex and medulla), adrenal cortex, hypothalamus, heart, lung, spleen, lymph nodes, and skeletal muscle. Each tissue sample was processed using three parallel preservation strategies to preserve structural, molecular, and ultrastructural information: fixation in 10% neutral-buffered formalin for histopathology, snap-freezing in liquid nitrogen for omics and biochemical analyses, and fixation in 2.5% glutaraldehyde for ultrastructural evaluation. Gross pathological findings were documented using a Leica DFC9000 macro-

imaging system to enable correlation with downstream microscopic analyses.

Histopathological processing and evaluation

Formalin-fixed tissues were processed using standard histological procedures, including graded dehydration, clearing, and paraffin embedding. Sections were cut at 4 µm thickness to balance cellular resolution and tissue architecture. Routine and special stains were applied to evaluate distinct pathological features: hematoxylin and eosin (H&E) staining for general morphology, Masson's trichrome staining for fibrosis and collagen deposition, periodic acid–Schiff staining for the assessment of tubular and basement membrane integrity, and Congo red staining to exclude amyloidosis in the context of chronic systemic disease.

Histopathological evaluation focused on morphological patterns consistent with toxicophysiological stress in metabolically active organs, particularly the liver and kidney (Mohammadzadeh *et al.*, 2025). Published reference data from healthy wild or captive felids were consulted, where available, to contextualize observed histopathological and biochemical alterations.

All slides were examined independently by a board-certified veterinary pathologist using a Leica DM6 B microscope, with systematic assessment of hepatic injury patterns (including steatosis, hepatocellular degeneration, and necrosis), renal tubular alterations, adrenal cortical cellular architecture, inflammatory cell distribution, vascular changes, and cytoplasmic inclusions.

Transmission electron microscopy

Transmission electron microscopy (TEM) was employed to assess subcellular alterations. Glutaraldehyde-fixed tissues were post-fixed with osmium tetroxide to enhance membrane contrast, dehydrated through a graded ethanol series, and embedded in epoxy resin. Ultrathin sections (approximately 70 nm) were prepared and examined using a JEOL JEM-1400 Plus transmission electron microscope.

The ultrastructural analysis focused on organelles relevant to PFAS-associated toxicophysiology, with particular attention to mitochondrial morphology, cristae organization, and membrane integrity. Additional features assessed included intramitochondrial vacuolization, peri-mitochondrial inclusions, autophagolysosome accumulation, and endothelial and tubular epithelial cell ultrastructural alterations. The presence of electron-dense crystalline or granular inclusions was also recorded, given the prior associations with high PFAS burden in other species (Mohammadzadeh *et al.*, 2022).

Quantitative PFAS profile

Tissue PFAS concentrations were quantified using ultra-high-performance liquid chromatography coupled with tandem mass spectrometry (UHPLC-MS/MS). Analyses were performed on a Thermo Scientific Vanquish ultrahigh-performance liquid chromatography system interfaced with a TSQ Altis triple quadrupole mass spectrometer. Sample preparation involved protein precipitation followed by solid-phase extraction (SPE) to minimize matrix interference and concentrate analytes. To ensure analytical accuracy and reproducibility, matrix-matched calibration curves and isotopically labeled internal standards were applied for each analyte (Pino *et al.*, 2020). Target compounds included PFOS, PFOA, PFHxS, PFNA, and PFDA, with results expressed as ng/g of wet tissue weight (w/w).

Spatial transcriptional mapping

Spatial gene expression profiling was conducted using the 10× Genomics Visium platform to preserve tissue architecture and regional transcriptional context. Fresh-frozen sections from the adrenal cortex, renal cortex, hepatic parenchyma, myocardium, and hypothalamus were cryosectioned at 10 µm thickness and mounted onto Visium slides. Sections were stained with hematoxylin and eosin and imaged using a Zeiss Axio Scan. Z1 slide scanner to generate high-resolution histological references.

Following tissue permeabilization, we generated spatially barcoded cDNA libraries according to the manufacturer's protocol and sequenced them on an Illumina NovaSeq 6000 platform. The raw sequencing data were processed using the Space Ranger software (v2.1) for alignment, barcode assignment, UMI counting, and spot-level expression matrices generation. Downstream analyses were performed using Seurat workflows, including SCTransform normalization to reduce technical variation, Harmony-based batch correction, and unsupervised clustering. Spatial transcriptional clusters were mapped back to histological features to identify microanatomical domains associated with molecular alterations.

Single-cell RNA sequencing

Single-cell transcriptomic profiling was performed to characterize cellular heterogeneity and identify cell populations exhibiting transcriptional alterations. To preserve cellular integrity and mitochondrial transcript content, tissue dissociation protocols were optimized for each organ using combined enzymatic and mechanical approaches (Yu and Miyamoto, 2021). The viability of single-cell suspensions exceeded 85% before library preparation. RNA integrity was assessed for all tissue samples, yielding RIN values between 7.2 and 8.5, indicating sufficient RNA quality for reliable single-cell transcriptomic analysis.

The libraries were generated using the Chromium Next GEM Single Cell 3' Kit v3.1 (10× Genomics) and sequenced on an Illumina NovaSeq 6000 S4 flow cell. Quality control filtering based on gene counts and mitochondrial transcript proportions excluded low-complexity cells and technical artifacts; however, mitochondrial transcript representation was evaluated cautiously, given the study's focus on mitochondrial dysfunction. To ensure that cells exhibiting potential mitochondrial stress or dysfunction were not

inadvertently excluded from our analysis, no strict threshold was applied to filter cells based solely on high mitochondrial transcript content. PCA and UMAP were used to reduce dimensionality, followed by unsupervised clustering and cell-type annotation through comparison with felid reference datasets and established marker genes.

Mitochondrial functional assays

Mitochondrial bioenergetic function was assessed using high-resolution respirometry with the Oroboros O2k system. Permeabilized myocardial and skeletal muscle fibers were analyzed to determine the maximal oxidative phosphorylation (OXPHOS) capacity across Complexes I–V, LEAK respiration as an indicator of proton conductance, and flux control ratios. Biochemical assays were performed to quantify oxidative stress markers, including malondialdehyde (MDA), protein carbonylation, and total antioxidant capacity, to complement functional measurements.

Targeted steroid hormone profiling (steroidomics)

Targeted steroid hormone profiling was performed to assess the adrenal endocrine function. Quantification was performed using a Sciex TripleTOF 6600+ hybrid mass spectrometer. The analytical panel included glucocorticoids (cortisol and corticosterone), mineralocorticoids (aldosterone), precursor steroids (e.g., pregnenolone), and intermediate metabolites within the adrenal steroidogenic pathway. To ensure analytical precision, hormone concentrations were normalized to tissue mass and quantified using isotopically labeled internal standards.

Immunohistochemical validation and spatial protein mapping

Immunohistochemistry was performed to validate transcriptional findings at the protein level and to assess spatial localization. Automated staining was performed using a Ventana BenchMark Ultraplatform. Primary antibodies targeted mitochondrial mass (TOMM20), autophagy (LC3B), immune checkpoint ligand (PD-L1), HIF-1α (hypoxia response), 8-OHdG (oxidative DNA damage), and steroidogenic enzymes CYP11B1 and CYP11B2. Antibody cross-reactivity with felid tissues was confirmed before the analysis.

We digitized and analyzed whole-slide images using QuPath v0.5 software to quantify staining intensity, subcellular localization, and spatial relationships between immunometabolic markers, enabling semi-quantitative and region-specific assessment (Kiran *et al.*, 2023).

Statistical analysis

All analyses were performed using the R software (v4.3.3). Given the single-specimen, exploratory nature of this study, all statistical analyses were performed for descriptive and hypothesis-generating purposes, not for inferential population-level conclusions. Accordingly, descriptive and exploratory statistical analyses were performed descriptively and exploratorily rather than for population-level inference. DESeq2 and single-cell modeling frameworks within Seurat or edgeR were used to conduct differential gene expression analyses to identify consistent directional changes in gene expression. Pathway enrichment analyses were performed using the ReactomePA package to highlight the biological processes that were affected. Summary statistics were reported for biochemical and respirometry data, and comparative tests were used cautiously to support descriptive interpretation rather than formal hypothesis testing.

Results

Gross and histopathological findings

Gross pathological examination revealed severe, multisystem alterations consistent with chronic toxicophysiological stress. During necropsy, the adrenal glands exhibited marked cortical thinning with loss of normal yellow lipid-rich appearance, accompanied by linear hemorrhagic streaks. The liver appeared pale and friable, with a mottled, mosaic-like cut surface, suggestive of heterogeneous parenchymal atrophy. The kidneys displayed a coarse, granular capsular surface with poor corticomedullary demarcation. The myocardium was diffusely pale with focal thinning. Although some post-mortem changes cannot be entirely excluded, the constellation and distribution of lesions were compatible with a chronic, systemic toxicophysiological stress pattern rather than acute agonal change (Fig. 1).

Histopathological evaluation further characterized these alterations. The hepatic parenchyma showed mixed microvesicular and macrovesicular steatosis, hepatocellular ballooning degeneration, and scattered acidophilic (Councilman-like) bodies. Hepatocellular mitochondria appeared swollen and structurally altered at higher magnification. Proximal tubular epithelial cells demonstrated prominent cytoplasmic vacuolation in the renal cortex, a feature commonly associated with toxic or metabolic stress. In addition, evidence of impaired mitophagic clearance was observed, accompanied by early IF changes. Adrenal cortical cells exhibited intensely eosinophilic cytoplasm with nuclear shrinkage and condensation, a pattern consistent with the functional exhaustion of steroidogenic cells previously described in endocrine-disruptive states (Sadek *et al.*, 2023) (Fig. 2).

Ultrastructural pathology

Transmission electron microscopy revealed extensive ultrastructural disruption across the affected organs. Hepatic and renal mitochondria displayed marked cristae loss (cristolysis), outer mitochondrial membrane rupture, and large intramitochondrial vacuoles. Distinct electron-dense crystalline inclusions were identified within the cytoplasm of renal proximal tubular cells. Mitochondrial cristae in adrenal cortical cells adopted aberrant tubular configurations, a morphology

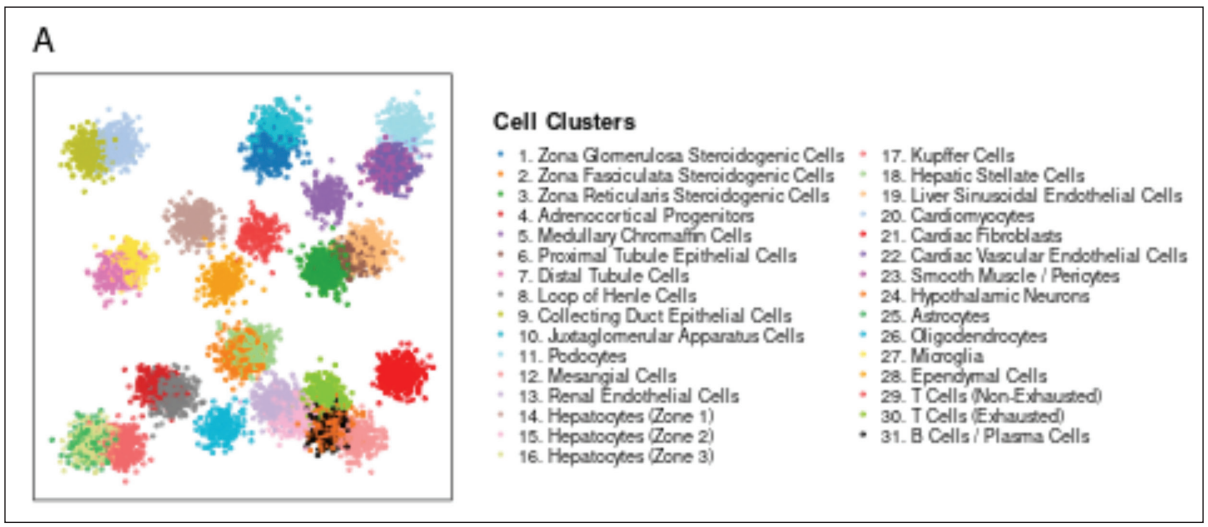


Fig. 1. Gross pathology of the liver, kidney, and adrenal gland in a Persian leopard (P. *pardus tulliana*) with documented PFAS accumulation. The adrenal gland shows cortical thinning, the liver displays a reticulated pattern, and the renal cortex appears granular. The findings are consistent with chronic toxicophysiological stress.

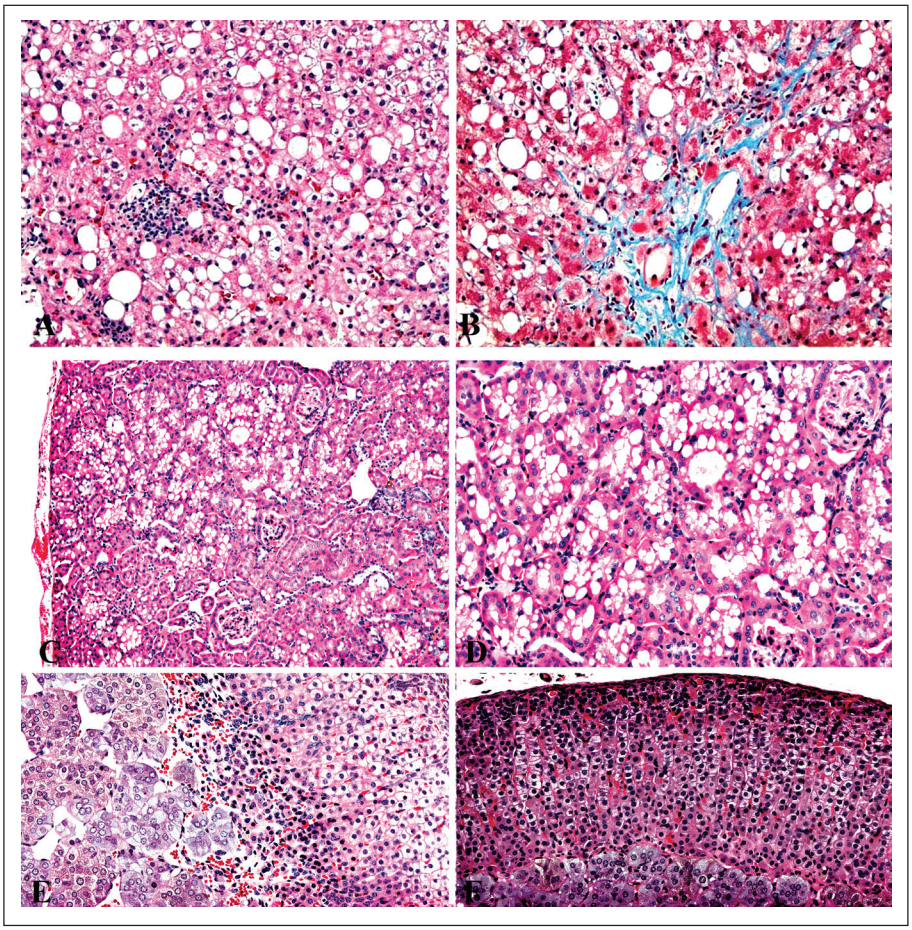


Fig. 2. Histopathology of multi-organ injury in a Persian leopard (*P. pardus tulliana*) with PFAS accumulation, hematoxylin and eosin staining, and Masson's trichrome staining The liver, kidney, and adrenal cortex show microvesicular steatosis, tubular vacuolation, and eosinophilia, respectively. These morphological alterations are consistent with the PFAS-associated injury patterns reported in other species.

previously associated with mitochondrial steroidogenic enzyme system inhibition under toxicological conditions (Isola *et al.*, 2013) (Fig. 3).

Quantitative analysis of PFAS tissue burdens

Quantitative chemical analysis demonstrated the presence of substantial PFAS tissue burden. UHPLC-MS/MS detected elevated PFOS, PFOA, and PFHxS concentrations across all examined organs. The adrenal gland exhibited particularly high PFOS concentrations (>320 ng/g wet weight), exceeding the values commonly reported in exposed wildlife species. Although species-specific toxic thresholds for large felids have not been established, this finding indicates a disproportionate accumulation within endocrine tissue (Table 1).

Table 1, quantitative analysis of perfluoroalkyl and polyfluoroalkyl substances (PFAS) in Persian leopard (*Panthera pardus tulliana*) tissues demonstrates widespread contamination with PFOS, showing the highest bioaccumulation across all organs. The adrenal cortex exhibited the greatest PFAS burden (430.5 ng/g), with PFOS concentrations exceeding 320 ng/g, consistent with the observed endocrine disruption. All values represent wet weight concentrations measured by ultra-high-performance liquid chromatography-MS/MS with isotopic dilution calibration.

Steroid hormone profiling

Targeted steroid hormone profiling revealed marked reductions in cortisol, corticosterone, aldosterone, and pregnenolone. These biochemical alterations are consistent with the profound impairment of adrenal steroidogenic capacity rather than physiological stress activation alone (Fig. 4). These hormone concentrations were compared to published reference ranges from healthy wild or captive felids where available, confirming that the observed reductions were outside physiological norms (Gomez-Sanchez *et al.*, 2017; Suski, 2020).

Spatial transcriptional mapping

Spatial transcriptomic analysis provided a molecular context for the observed pathology. Gene networks involved in oxidative phosphorylation (OXPHOS), mitochondrial ribosomal function, and steroid biosynthesis showed coordinated downregulation in the adrenal cortex, renal cortex, myocardium, and hypothalamus. These metabolically suppressed regions were spatially juxtaposed to inflammatory microdomains characterized by elevated IL-18, TNF, and CCL20 expression. This spatial coupling of metabolic dysfunction and localized inflammation is a recognized feature associated with exposure to mitochondrial toxicants (Fig. 5).

Single-cell transcriptomics

Single-cell RNA sequencing further resolved cell-type–specific transcriptional alterations. Thirty-one distinct transcriptional clusters were identified across the examined tissues. Steroidogenic cell populations demonstrated pronounced downregulation of transcripts

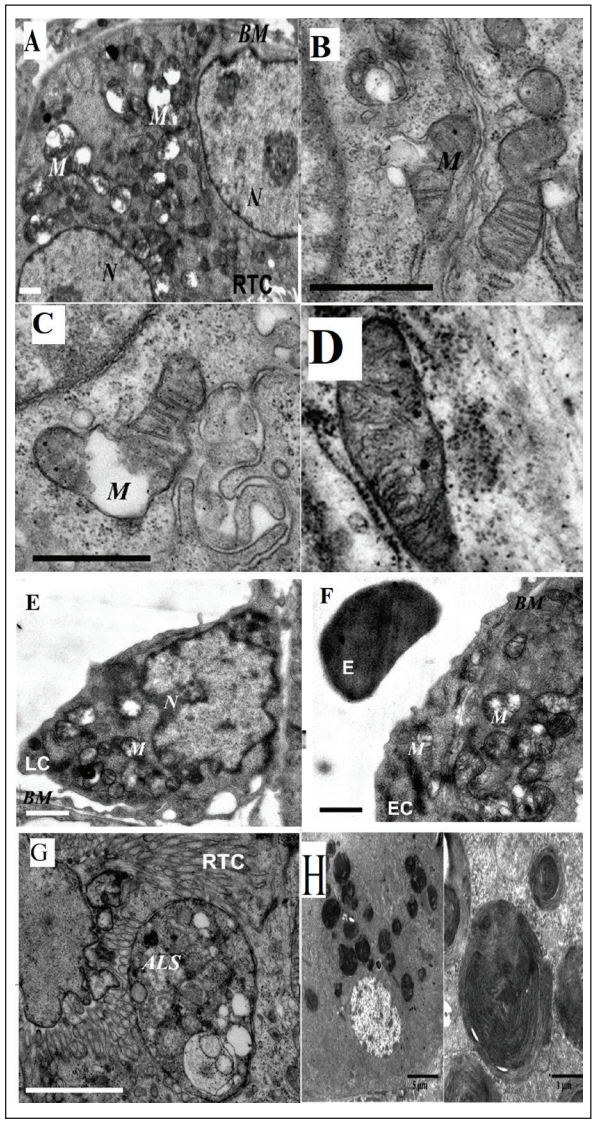


Fig. 3. Ultrastructural changes in renal cells from a Persian leopard *(Panthera pardus tulliana*) with PFAS accumulation in a mouse model (A–D, G) Severe mitochondrial damage, including cristolysis, membrane rupture, and swelling, in renal tubular epithelial cells (E) A leukocyte with swollen mitochondria. (F) Mitochondrial injury of the glomerular endothelium. (H) Electron-dense cytoplasmic inclusions in a proximal tubular epithelial cell, suggestive of high PFAS burden-associated abnormal intracellular accumulations. Abbreviations: M, damaged mitochondria; BM, basal membrane; N, nucleus; ALS, autophagolysosome; E, erythrocyte. Scale bar, 1 μm (A–G). Scale bar for H, 500 nm.

encoding OXPHOS Complex I and V subunits, which is concordant with TEM-observed ultrastructural mitochondrial damage. Immune cell clusters exhibited increased expression of inhibitory immune checkpoint receptors, including PDCD1 (PD-1), LAG3, and TIGIT, suggesting an exhausted immune phenotype.

Table 1. Quantitative PFAS tissue burdens (ng/g wet weight) in organs of the Persian leopard (*P. pardus tulliana*).

Organ	PFOS	PFOA	PFHxS	PFNA	PFDA	Total PFAS
Adrenal Cortex	325.4	45.2	38.7	12.3	8.9	430.5
Liver	287.6	52.8	42.3	15.7	12.4	410.8
Kidney Cortex	245.8	38.9	35.2	11.2	7.8	338.9
Myocardium	156.3	28.4	22.1	8.6	5.3	220.7
Hypothalamus	132.7	24.8	18.9	7.2	4.1	187.7
Spleen	198.5	32.7	28.4	9.8	6.5	275.9
Lung	167.2	29.5	24.3	8.9	5.7	235.6
Skeletal Muscle	89.6	18.3	12.7	5.4	3.2	129.2

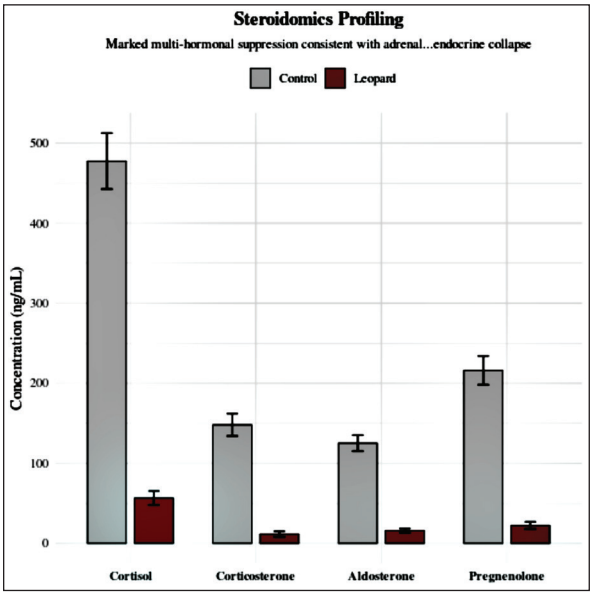


Fig. 4. Steroidomics profiling reveals adrenal–endocrine suppression in a Persian leopard (*P. pardus tulliana*) with PFAS accumulation Targeted LC–MS/MS steroid panel demonstrates marked reductions in cortisol, corticosterone, aldosterone, and pregnenolone levels. This pattern is consistent with the broad impairment of adrenal steroidogenic capacity associated with PFAS interference with cholesterol transport, mitochondrial steroidogenic enzymes, and downstream glucocorticoid and mineralocorticoid synthesis.

Cardiomyocyte clusters displayed altered expression of sarcomeric genes (MYH7B and TNNT2) and reduced activity within the PGC-1α–regulated mitochondrial biogenesis program (Fig. 6).

Immunohistochemical validation

Immunohistochemical analysis corroborated the key transcriptomic findings at the protein level. TOMM20 immunoreactivity was reduced in renal and hepatic tissues, indicating decreased mitochondrial mass. Aberrant LC3B staining patterns were consistent with histologically observed impaired mitophagic flux. PD-L1 expression was increased in immune cells, renal tubular epithelium, and perivascular macrophages, indicating the presence of a localized immunoregulatory milieu. Quantitative image analysis demonstrated a 3.4-fold increase in nuclear HIF-1α and a 2.8-fold increase in the oxidative DNA damage marker 8-OHdG, consistent with widespread hypoxic stress and redox imbalance (Fig. 7).

Mitochondrial functional assays and biomarkers of oxidative stress

Functional bioenergetic assays confirmed severe mitochondrial dysfunction. High-resolution respirometry of permeabilized muscle fibers revealed a 57% reduction in maximal OXPHOS capacity, a 41% increase in LEAK respiration, and a marked reduction in the respiratory control ratio, indicating profound mitochondrial uncoupling. These functional deficits were paralleled by a 2.9-fold elevation in hepatic MDA levels relative to established reference ranges, consistent with systemic lipid peroxidation and oxidative stress (Table 2).

Table 2 mitochondrial functional assessment reveals severe bioenergetic compromise in tissues of the Persian leopard (*P. pardus tulliana*) OXPHOS capacity was reduced by 57% with a 41% increase in LEAK respiration, indicating uncoupled mitochondrial respiration. The respiratory control ratio collapse (70% reduction) demonstrates a profound impairment of mitochondrial coupling efficiency. Oxidative stress biomarkers show marked elevation, with approximately 2.9-fold increase in MDA, protein carbonylation increased approximately 2.9-fold, and 8-hydroxy-2'-deoxyguanosine (8-OHdG) increased 2.5-fold, consistent with systemic redox imbalance. Reference values were derived from healthy felid controls.

Discussion

To the best of our knowledge, this study provides the first integrative, multi-scale pathological and molecular characterization of PFAS-associated multi-organ dysfunction in an endangered apex predator. By

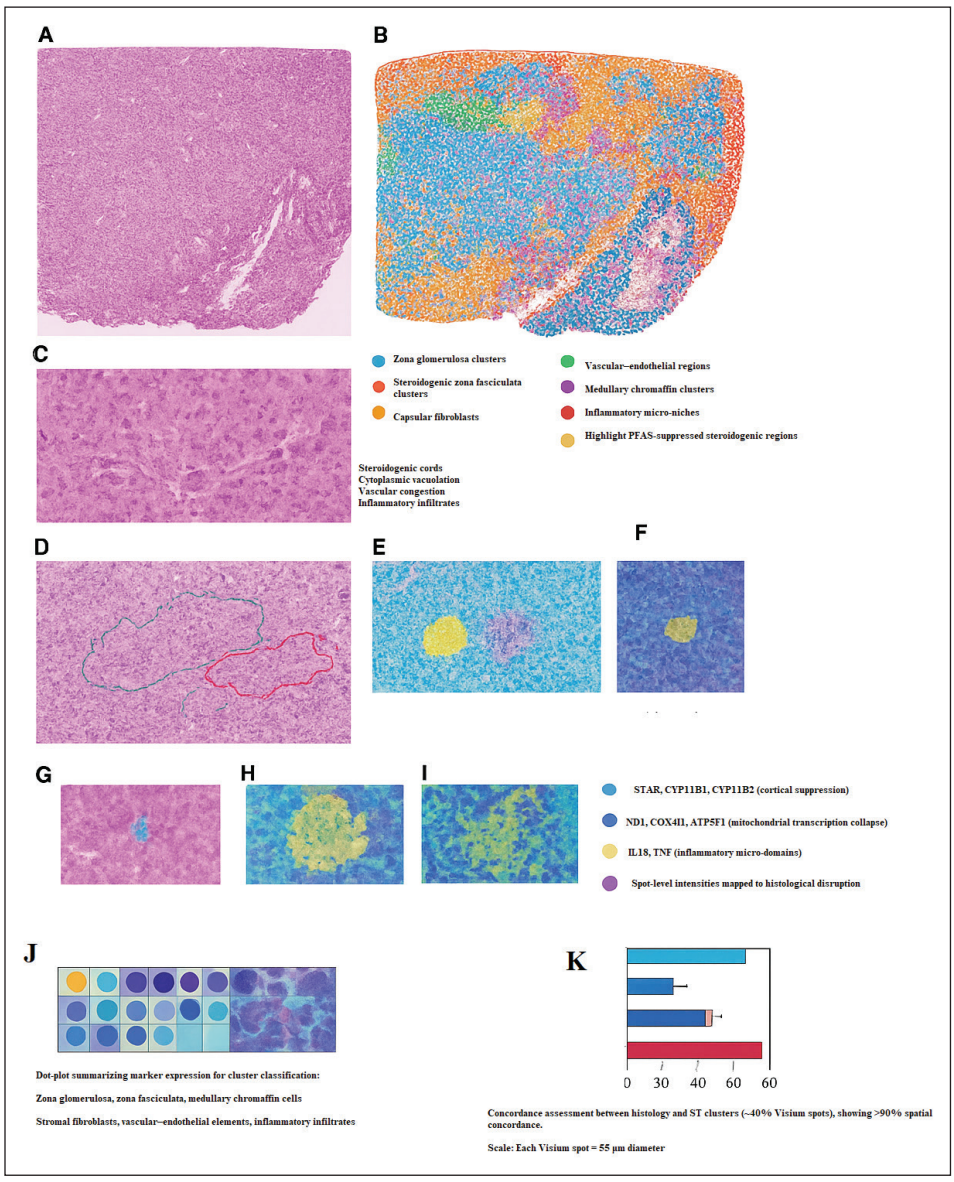


Fig. 5. Spatial transcriptomic mapping of adrenal cortical injury in a Persian leopard (*P. pardus tulliana*) with PFAS accumulation (A) Hematoxylin and eosin staining of the adrenal cortex shows thinning, pale cytoplasm, disrupted zona fasciculata architecture, and focal hemorrhage. (B) Unsupervised spatial transcriptomic clusters mapped onto the adrenal section, revealing cortical regions, including zona glomerulosa clusters, steroidogenic zona fasciculata clusters, capsular stromal fibroblasts, vascular regions, medullary chromaffin clusters, and inflammatory foci. Areas with steroidogenic pathway transcriptional suppression appear as clusters with reduced gene expression. (C) High-magnification images highlight adrenal features, including residual steroidogenic cords, cytoplasmic vacuolation, vascular congestion, and inflammatory cell infiltration. (D) Annotated adrenal section delineating preserved and damaged steroidogenic zones, vascular regions, and inflammatory cell aggregates. (E) Transcriptomic clusters projected onto annotated histology, demonstrating molecular identity and tissue architecture concordance. (F–I) Spatial expression patterns for STAR, CYP11B1, and CYP11B2 show reduced expression in affected areas associated with PFAS. ND1, COX4I1, and ATP5F1 reduced the expression of mitochondrial genes. IL18 and tumor necrosis factor demarcate inflammatory microdomains. (J) Dot plot summarizing the expression of molecular markers used for cluster classification, confirming the separation of ZG, ZF, medullary chromaffin cells, stromal fibroblasts, vascular cells, and inflammatory cells. (K) Comparison between histology and transcriptomic cluster identity across five random adrenal areas (approximately 40% of Visium spots) demonstrates >90% spatial concordance, confirming a strong correlation between molecular identity and adrenal tissue architecture. Each Visium spot is 55 µm in diameter.

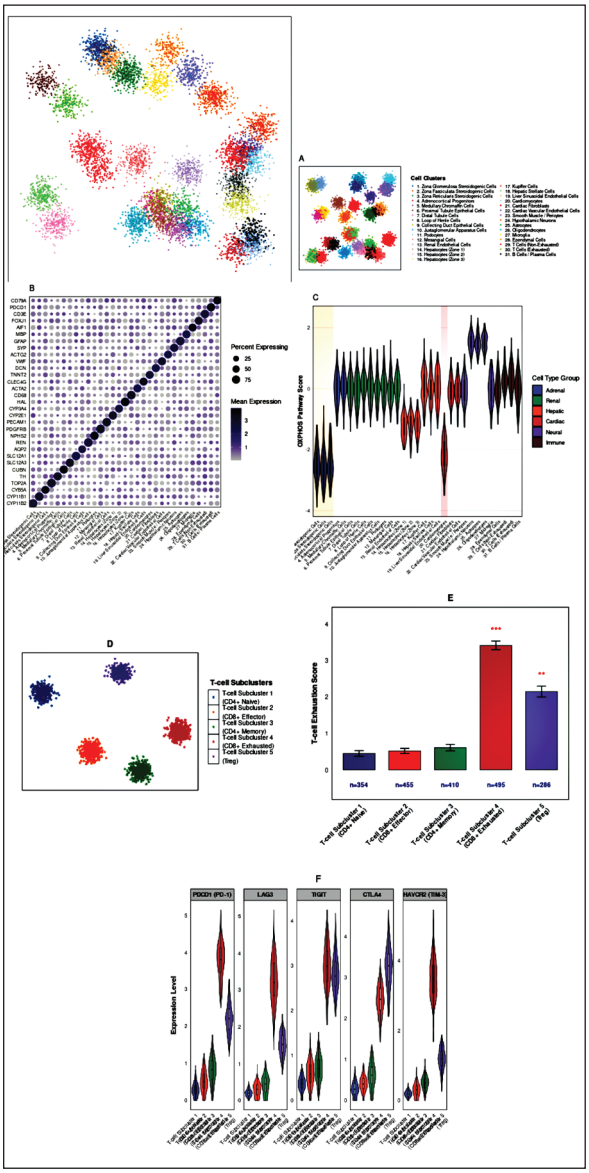


Fig. 6. Multi-modal evidence of mitochondrial dysfunction, steroidogenic suppression, and T-cell exhaustion in a Persian leopard (*P. pardus tulliana*) with PFAS accumulation (A) UMAP showing 31 single-cell clusters from the adrenal cortex, myocardium, renal cortex, liver, and hypothalamus. (B) Dot plot displays marker gene expression for cluster annotation, with color indicating mean expression and size indicating percentage of cells expressing each marker. (C) Violin plot showing the OXPHOS pathway activity scores in major cell types, with steroidogenic cells showing reduced scores. (D) UMAP illustrating five T-cell subclusters. (E) Bar plot showing the average T-cell exhaustion score per subcluster. (F) Violin plots showing inhibitory receptor expression (PDCD1, LAG3, TIGIT, CTLA4, and HAVCR2) across T-cell subclusters, suggesting an exhausted immune phenotype. Statistical annotations indicate significance based on the Wilcoxon test with correction for multiple comparisons.

combining gross pathology, ultrastructural analysis, spatial and single-cell transcriptomics, steroid metabolomics, and functional bioenergetic assays, we delineated a coherent mechanistic framework consistent with a link between environmental PFAS accumulation and mitochondrial failure, endocrine disruption, and subsequent immunometabolic exhaustion.

The extensive mitochondrial injury observed across multiple organs is consistent with the experimental evidence that PFOS and PFOA can destabilize mitochondrial membranes and impair oxidative phosphorylation (Bonato *et al.*, 2020; Hofmann *et al.*, 2023). In particular, the pronounced adrenal involvement—reflected by disproportionate PFAS accumulation and zonal transcriptional suppression—parallels findings in rodent and NHP models. These effects have been attributed to the interference of PFAS with the steroidogenic acute regulatory (StAR) protein and the distinctive lipid composition of steroidogenic mitochondrial membranes (Kumar, 2024; Rigoli, 2024). Correspondingly, the marked suppression of cortisol, corticosterone, and aldosterone mirrors hormonal alterations reported in PFAS-exposed mammals, reinforcing an association between PFAS burden and impaired endocrine homeostasis (Gomez-Sanchez *et al.*, 2017; Mukai *et al.*, 2021).

At the ultrastructural level, hepatic and renal mitochondrial abnormalities—including cristae disruption and intramitochondrial inclusions—closely resemble lesions described in PFAS toxicity studies in murine, piscine, and avian models (Piva *et al.*, 2022; Kaye, 2024; Kam *et al.*, 2025). Dense crystalline inclusions within renal proximal tubular cells are particularly noteworthy. Such inclusions are uncommon outside specific toxic or storage-related conditions and are compatible with emerging hypotheses that PFAS may form stable complexes with intracellular proteins, potentially contributing to tubular dysfunction (Fenton *et al.*, 2021; Yang *et al.*, 2023). These findings suggest heightened susceptibility of apex felids to chronic PFAS accumulation in the context of trophic biomagnification, although species-specific toxicity thresholds remain undefined.

Spatial transcriptomic profiling revealed a striking spatial juxtaposition of metabolically quiescent regions and inflammatory microdomains. Moreover, inflammatory microdomains were identified. This architectural pattern aligns with contemporary toxicological models in which localized fibro-inflammatory remodeling is accompanied by mitochondria-associated cellular stress (Polonsky *et al.*, 2024; Battat *et al.*, 2025). Such spatial heterogeneity may underlie the uneven functional decline observed within the affected organs.

A prominent systemic finding was evidence of immune reprogramming. The transcriptional signature of T-cell exhaustion—characterized by the upregulation of PD-1, LAG-3, and TIGIT—is consistent with the patterns reported in chronic inflammatory and toxicant-

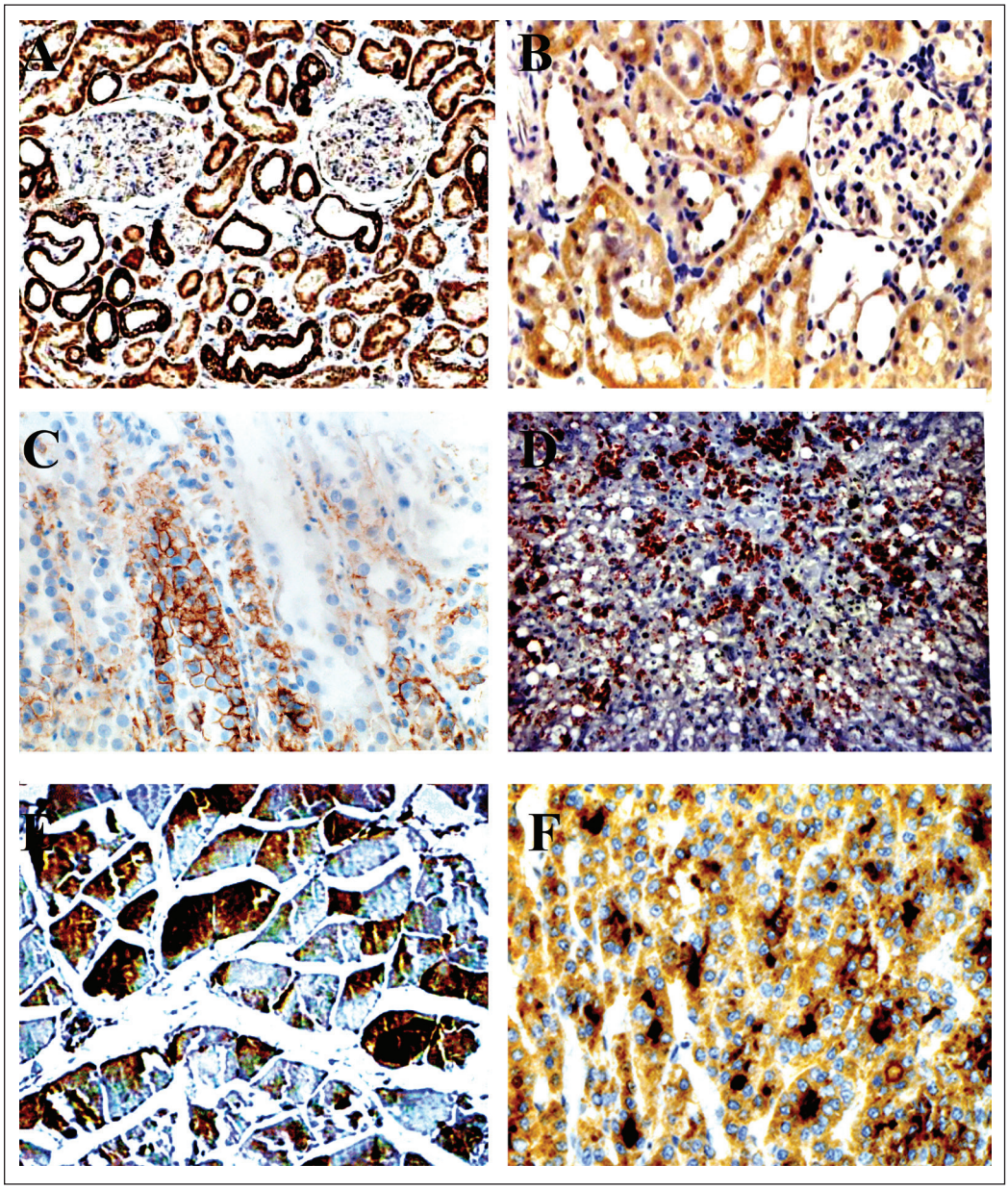


Fig. 7. Immunohistochemical mapping of mitochondrial mass reduction, autophagic arrest, and immune checkpoint expression in a Persian leopard (*P. pardus tulliana*) with PFAS accumulation in a mouse model (A) TOMM20 staining reveals reduced mitochondrial mass in the renal tubular epithelium. (B) LC3B staining in renal tubules is consistent with impaired mitophagic flux. (C) PD-L1 expression in renal tubular epithelium and perivascular macrophages, supporting localized immunoregulatory milieu. (D) Nuclear HIF-1α stabilization in centrilobular hepatocytes and cardiomyocytes, consistent with hypoxic stress. (E) 8-OHdG nuclear staining of hepatocytes, indicating oxidative DNA damage. Scale bars: 50 μm.

exposed states (Kgokolo *et al.*, 2022; Jantz-Naeem *et al.*, 2023). Although causality cannot be established, these findings are compatible with the possibility that chronic exposure to environmental toxicants may recalibrate immunometabolic setpoints. From a conservation medicine perspective, such immune exhaustion could plausibly increase susceptibility to endemic infections and inflammatory conditions, thereby amplifying population-level vulnerability.

Similarly, coordinated downregulation of MYH7B, TNNT2, and PGC-1α-associated pathways in cardiomyocytes provides a plausible molecular context for PFAS-associated cardiotoxicity previously reported in experimental systems (Vainshtein *et al.*,

Table 2. Mitochondrial functional assays and biomarkers of oxidative stress in Persian leopard (*Panthera pardus tulliana*) tissues.

Parameter	Cardiac Muscle	Skeletal Muscle	Liver	Reference Values	% Change
Mitochondrial function					
OXPHOS capacity (pmol O_2/s/mg)	84.3	92.7	-	196.5 ± 15.2	-57.1%
LEAK respiration (pmol O_2/s/mg)	45.6	51.2	-	32.3 ± 4.1	+41.2%
Respiratory control ratio	1.85	1.81	-	6.08 ± 0.45	-69.6%
Complex I activity (%)	42.7	45.3	-	100 ± 8.5	-56.5%
Complex IV activity (%)	38.9	41.6	-	100 ± 7.2	-60.3%
Oxidative stress markers					
MDA (nmol/mg protein)	-	-	18.7	6.4 ± 1.2	+192.2%
Protein carbonylation (nmol/mg)	12.3	10.8	15.6	4.2 ± 0.8	+193.5%
Total antioxidant capacity (μM)	1.24	1.31	0.87	2.85 ± 0.34	-56.1%
8-OHdG (ng/μg DNA)	3.45	3.12	4.28	1.53 ± 0.28	+125.5%

2015; Qi *et al.*, 2023). These findings further support mitochondrial dysfunction as a central pathological feature associated with multisystem physiological dysregulation when interpreted alongside elevated systemic oxidative stress markers, including MDA and 8-OHdG (Wu *et al.*, 2004; Pagano *et al.*, 2014). This interpretation reflects the convergence of structural, biochemical, and transcriptomic evidence rather than definitive causal attribution.

Study limitations and alternative explanations

Several important limitations must be acknowledged. This investigation is based on a single individual and a cross-sectional design, without population-level reference data for baseline PFAS exposure or transcriptomic states. The absence of longitudinal sampling and internal controls further constrains causal inference. Accordingly, the definitive causal attribution of all observed pathological findings solely to PFAS exposure is not possible.

Several alternative or contributory factors should be considered. First, the estimated age of the individual (>10 years) raises the possibility of age-related degenerative changes, particularly in mitochondrial function and steroidogenic capacity. Second, although no active infectious process was identified on comprehensive histopathological screening, subclinical or resolved infections cannot be excluded. Third, nutritional stress—common in fragmented leopard populations—may independently induce hepatic steatosis, immunosuppression, and endocrine alterations. Fourth, the potential contribution of co-occurring environmental pollutants (e.g., heavy metals and organochlorines) was not quantified and may exert additive or synergistic effects.

Therefore, while the findings delineate a plausible mechanistic framework, they should be interpreted as a detailed molecular and pathological characterization of a single PFAS-exposed individual, rather than establishing definitive causation, generating hypotheses for future controlled or population-level investigations.

Conclusion

In conclusion, this study provides a multi-level characterization of molecular and pathological features consistent with PFAS-associated pharmacophysiological failure in a threatened apex predator. By integrating classical pathology with ultrastructural, spatial transcriptomic, single-cell, steroidomic, and functional bioenergetic analyses, we propose a unified pathophysiological framework in which mitochondrial disruption is a central pathological feature associated with endocrine impairment and widespread immunometabolic dysregulation.

Mitochondrial dysfunction emerged as a recurring molecular and structural pattern across examined organs and was associated with AD, impaired energy production, immune dysregulation, and systemic redox imbalance. Collectively, these findings suggest that trophic biomagnification makes apex felids particularly susceptible to persistent organic pollutants, although confirmation requires population-level investigation.

From a conservation and environmental health perspective, PFAS contamination may impose both overt and subclinical fitness costs on wild Persian leopard (*P. pardus tulliana*) populations. Endocrine disruption, attenuated stress responsiveness, immune exhaustion, and reduced energetic capacity could compromise survival, reproductive success, and long-term population resilience. Importantly, the multimodal analytical strategy employed here demonstrates how substantial mechanistic insight can be derived from limited biological material in rare and endangered species.

This work should be regarded as a descriptive, hypothesis-generating case study that bridges the

fields of experimental toxicology and conservation medicine. Future priorities include expanded PFAS biomonitoring, non-invasive longitudinal endocrine assessments, and comparative experimental models to define susceptibility thresholds in terrestrial apex predators.

Acknowledgments

The authors would like to thank the Department of Environment of Iran for their cooperation in sample collection. The authors also acknowledge the technical support provided by the Laleh pathology laboratory.

Authors' contributions

Peyman Mohammadzadeh: Conceptualization, Methodology, Investigation, Original Draft Writing, Review and Editing. Mohammad Reza Salim Bahrami: Formal analysis, investigation, data collection, and visualization. Farshad Ziaee: Validation, Resources, and Project Administration. Arshia Dousti: Investigation and formal analysis. Amin Pilvaieh: Investigation and data collection.

Conflict of interest

The authors have no conflicts of interest to declare.

Funding

This research did not receive any specific grant from public, commercial, or not-for-profit funding agencies.

Data availability

The datasets generated and analyzed during the current study are available upon reasonable request from the corresponding author.

References

Battat, R., Sangiorgi, B., Linggi, B., Gui, X., Smith, M.I., Mehandru, S., Longman, R., Lukin, D.J., Scherl, E.J., Qin, L., Ma, C., Teft, W. and Vande Casteele, N. 2025. Spatial transcriptomics reveals unique inflammatory signatures across all anatomic locations in postoperative Crohn's disease. J. Crohns. Colitis. 19(10), jjaf180.

Bonato, M., Corrà, F., Bellio, M., Guidolin, L., Tallandini, L., Irato, P. and Santovito, G. 2020. Int . J. Environ. Res. Public Health 17, 8020.

de Paula Nunes, E., Pestana, B.A.D. and Pereira, B.B. 2025. J. Toxicol . Environ. Health B Crit. Rev. [In press].

Fenton, S.E., Ducatman, A., Boobis, A., DeWitt, J.C., Lau, C., Ng, C., Smith, J.S. and Roberts, S.M. 2021. Per- and Polyfluoroalkyl substance toxicity and human health review: current state of knowledge and strategies for informing future research. Environ. Toxicol. Chem. 40(3), 606–630.

Fritsche, K., Ziková-Kloas, A., Marx-Stoelting, P. and Braeuning, A. 2023. Int. J. Mol. Sci. 24, 2686.

Ghoddousi, A.R., Bleyhl, B.E., Askerov, E.L., Heidelberg, A.U., Kabir, M.U., Lortkipanidze, B.E., Manvelyan, K.A., Mengüllüoğlu, D., Moheb, Z., Mousavi, M. and Pkhitikov, A.L. 2022. Cat News Spec. Iss. 15:61–66.

Gomez-Sanchez, C.E., Qi, X., Gomez-Sanchez, E.P., Sasano, H., Bohlen, M.O. and Wisgerhof, M. 2017. Mol. Cell. Endocrinol. 439, 74–80.

Hofmann, A., Mishra, J.S., Yadav, P., Dangudubiyyam, S.V., Blesson, C.S. and Kumar, S. 2023. J. Environ. Sci. Public Health 7, 164.

Isola, R., Solinas, P., Concettoni, C., Atzeni, F., Loy, F., Diana, M., Isola, M., Giacchetti, G., Boscaro, M., Riva, A. and Mariotti, S. 2013. Cell Tissue Res. 351:409-417.

Jantz-Naeem, N., Böttcher-Loschinski, R., Borucki, K., Mitchell-Flack, M., Böttcher, M., Schraven, B., Mougiakakos, D. and Kahlfuss, S. 2023. TIGIT signaling and its influence on T cell metabolism and immune cell function in the tumor microenvironment. Front. Oncol. 13, 1060112.

Kam, Y., Winer, L. and Romero, N. 2025. Front. Toxicol. 7, 1582891.

Kaye, E. 2024. Mechanistic Approach to Understanding Adverse Liver Outcomes Related to PFAS Exposure in Neonatal and Adult Mice. M.S. Thesis, University of Rhode Island, Kingston, RI.

Kgokolo, M.C.M., Anderson, K., Siwele, S.C., Steel, H.C., Kwofie, L.L.I., Sathekge, M.M., Meyer, P.W.A., Rapoport, B.L. and Anderson, R. 2022. Front. Oncol. 12:819790.

Kiran, N., Sapna, F., Kiran, F., Kumar, D., Raja, F., Shiwlani, S., Paladini, A., Sonam, F., Bendari, A., Perkash, R.S., Anjali, F. and Varrassi, G. 2023. Cureus. Cureus 15, e44620.

Kumar, S. 2024. Perfluorooctane sulfonic acid (PFOS), Hypertensive Disorders of Pregnancy (HDP), and Offspring Health: A Mechanistic Investigation. Ph. D. Thesis. p. 115.

Marlatt, V.L., Bayen, S., Castaneda-Cortès, D., Delbès, G., Grigorova, P., Langlois, V.S., Martyniuk, C.J., Metcalfe, C.D., Parent, L., Rwigemera, A. and Thomson, P. 2022. Environ. Res. 208, 112584.

Mohammadzadeh, P., Rasuli, A., Gorgani, B.N. and Mohammadi, S. Clinical and histopathological findings associated with ataxic myoglobinuric syndrome in Persian onager (*Equus hemionus onager*). In Proc. 5th Int. Vet. Pathol. Congr.,2022 Tehran, Iran, pp 238–251.

Mohammadzadeh, P., Ziaee, F. and Mousavi, F. 2025. Open. Vet. J. 15, 4763–4771.

Mukai, K., Sugimoto, H., Kamiya, K., Suzuki, R., Matsuura, T., Hishiki, T., Shimada, H., Shiro, Y., Suematsu, M. and Kagawa, N. 2021. Spatially restricted substrate-binding site of cortisol-synthesizing CYP11B1 limits multiple hydroxylations and hinders aldosterone synthesis. Curr. Res. Struct. Biol. 3, 192–205.

Naderi, M., Farashi, A. and Erdi, M.A. 2018. PLoS One. 13:e0195387.

Namroodi, S., Hoseini, S.M., Alijani, H., Amani, R. and Roshanian, S. 2019. A case report of

dermatofibroma in a Persian leopard in Golestan National Park, Iran. J. Wildl. Dis. 55, 975–978.
Pagano, G., Talamanca, A.A., Castello, G., et al. 2014. Oxid. Med. Cell. Longev. 2014:541230.
Pino, L.K., Searle, B.C., Yang, H.Y., Hoofnagle, A.N., Noble, W.S., MacCoss, M.J. 2020. J. Proteome Res. 19, 1147–1153.
Piva, E., Schumann, S., Bonato, M., Bertotto, D., Marion, A., Irato, P. and Santovito, G. 2022. J. Biol. Res. 95, 15–16.
Polonsky, M., Gerhardt, L.M.S., Yun, J., Koppitch, K., Colón, K.L., Amrhein, H., Wold, B., Zheng, S., Yuan, G.C., Thomson, M., Cai, L. and McMahon, A.P. 2024. Spatial transcriptomics defines injury specific microenvironments and cellular interactions in kidney regeneration and disease. Nat. Commun. 15(1), 7010.
Qi, X.M., Qiao, Y.B., Zhang, Y.L., Wang, A.C., Ren, J.H., Wei, H.Z. and Li, Q.S. 2023. PGC-1α/NRF1-dependent cardiac mitochondrial biogenesis: A druggable pathway of calycosin against triptolide cardiotoxicity. Food Chem. Toxicol. 171, 113513.
Rigoli, M.T. 2024. The interplay between endocrine disruption and genetics in the physiopathology of human neurodevelopment: bridging epidemiology to molecular insights through brain organoids and high resolution OMIC modelling. Ph. D. Thesis.
Sadek, D.R., Abunasef, S.K. and Khalil, S. 2023. J. Microsc. Ultrastruct. 13, 16–24.
Sarri, N., Druid, H., Rezaie, A.R., Osinga, K., Sultana, N. and Alkass, K. 2025. Biomolecules 15, 1483.
Schwarzlmueller, P., Triebig, A., Assié, G., Jouinot, A., Theurich, S., Maier, T., Beuschlein, F., Kobold, S., Kroiss, M. 2025. Nat. Rev. Endocrinol. [In press].
Suski, J. 2020. Investigating potential risk to threatened and endangered species from per-and polyfluoroalkyl substances (PFAS) on department of defense (DoD) sites. Ph. D. Thesis, Oregon State Univ., Corvallis, OR.
Taher, H. and Lohmann, R. 2025. Environ. Sci. Technol. [In press].
Vainshtein, A., Desjardins, E.M., Armani, A., Sandri, M., Hood, D.A. 2015. Skelet. Muscle. 5:9.
Wu, L.L., Chiou, C.C., Chang, P.Y. and Wu, J.T. 2004. Clin. Chim. Acta. 339, 1–9.
Yang, Y., Wang, H., Kouadir, M., Song, H. and Shi, F. 2019. Recent advances in the mechanisms of NLRP3 inflammasome activation and its inhibitors. Cell Death Dis. 10(2), 128.
Yu, J.D. and Miyamoto, S. 2021. Cells. Cells 10, 3330.